IEEE Open Journal of
Industry Applications

Received 23 August 2020; revised 6 October 2020; accepted 26 October 2020. Date of publication 29 October 2020;
date of current version 9 November 2020. The review of this article was arranged by Editor Dr. S. Doolla.

Digital Object Identifier 10.1109/OJIA.2020.3034608

Deep Learning for Hardware-Based Real-Time Fault Detection and Localization of All Electric Ship MVDC Power System

QIN LIU [1] (Student Member, IEEE), TIAN LIANG [2] (Member, IEEE), AND VENKATA DINAVAHI [2] (Fellow, IEEE)

[1]School of Mechanical, Electronic and Control Engineering, Beijing Jiaotong University, Beijing 100044, China
[2]Department of Electrical and Computer Engineering, University of Alberta, Edmonton, Alberta T6G 2V4, Canada

CORRESPONDING AUTHORS: QIN LIU; TIAN LIANG (e-mail: qin9@ualberta.ca; tliang5@ualberta.ca)

This work was supported by the Natural Science and Engineering Research Council of Canada (NSERC). The work of QIN LIU was supported by China Scholarship Council (CSC).

ABSTRACT The tendency toward electrification of marine vessels has led the evolution of the all electric ship (AES). The harsh operating environment of the AES makes the shipboard power system (SPS) vulnerable, so a powerful monitoring system for fault detection and localization (FDL) is essential for safe navigation. We propose a machine learning based FDL method for monitoring the system condition with the problem of imbalanced training dataset. The generative adversarial network (GAN) comprising of deep convolutional neural networks was employed to synthesize numerous valid samples. Feature extraction and selection technologies were applied to time-series signals to reduce features for monitor training. Finally, the random forest (RF) model was trained using the augmented training dataset, combining real data with generated ones by GAN, to verify the capability of the GAN-RF based FDL method. Both real training and testing data were collected from the SPS model established in PSCAD/EMTDC. The results demonstrated that the monitor could distinguish different conditions in real-time with the help of hardware implementation on the FPGA and a 99% classification accuracy was achieved with excellent anti-noise capability.

INDEX TERMS All electric ship, correlation based feature selection, deep convolutional neural networks, fault detection and localization, field-programmable gate array, generative adversarial networks, multivariate empirical mode decomposition, mediumvoltage direct current, machine learning, random forest, real-time systems.

I. INTRODUCTION

Since human beings intended to explore land that had not been set foot on, marine transportation has been an indispensable tool to know about and communicate with the world. The tendency toward electrification of ocean-going vessels leads to an evolution to the all electric ship (AES). Conventional architectures of the shipboard power system (SPS) are medium-voltage AC (MVAC) and low-voltage DC (LVDC). Nowadays, the improvement of thermal, mechanical and insulated properties of high-voltage DC equipment pushes forward the development of medium-voltage DC (MVDC) distribution networks (i.e. 1kV-35kV [1]) for the AES [2], [3]. MVDC SPS provides a promising solution for significantly higher power demand of the AES, since lower currents need to be handled than LVDC as well as bulky low-frequency transformers and phase angle synchronizers are eliminated compared with MVAC [1]. However, the electrification system on AES is more vulnerable than terrestrial systems due to harsh environment at sea and the requirement of switching between different voyage modes. Even a minor fault among myriad components of the SPS may result in a catastrophe; thus a powerful monitoring system for fault detection and localization (FDL) of AES is crucial for safe navigation.

Machine learning has become a hot spot for dealing with FDL problems in the maritime industry [4]. In [5] a deep learning network has been designed to classify different faults

in rolling bearings of ship borne antenna according to the extracted features by multiscale inner product. Bayesian inference have been adopted for diagnosis diesel engine faults in [6]. Fault detection and health monitoring for the ship propulsion system has been researched based on the support vector machine (SVM) [7]. Reference [8] combined random forest (RF) algorithm with the shuffled frog leaping algorithm (SFLA) in order to locate the rudder fault. To the best of the authors' knowledge, few works have been reported to monitor and detect the faults may occur in the entire SPS of an AES.

To efficiently take advantage of the valuable data, feature selection and extraction which pick out a representative set of features for constructing a best-matched machine learning model are significant steps in the data preprocessing. Empirical mode decomposition (EMD) is one of the popular signal-processing methods. It has been widely applied in the fault diagnosis field [9]–[13], since the information of both time and frequency domain can be obtained from a series of intrinsic mode functions (IMFs) decomposed by EMD. For detecting multiple fault types of the AES, multichannel signals are sampled from various components of the power system. The traditional EMD can only decompose the signals one by one with different decomposition scales [14]. Multivariate empirical mode decomposition (MEMD) was developed [15] as an extension of EMD to solve the mode-mixing issue for multichannel signals. The information fusion between different channels are considered by MEMD that can align common frequency modes across channels in same index IMFs. After extracting temporal and spectral statistic characteristics using MEMD, features for establishing the model can be further decreased by selecting a feature subset that contains features highly correlated with the prediction, yet uncorrelated with each other [16]. Filter methods estimate the worth of features using heuristics directly from data. They are proved to perform similar to but execute considerably faster than the wrapper methods that estimate the worth of features according to the learning algorithm [17]–[19]. In this work, we adopt a filter named correlation based feature selection (CFS) method.

There is one more challenge for industrial fault detection using machine learning methods which highly rely on the data collected from real-world application scenarios. The data of faulty conditions are far fewer than for the normal conditions, i.e. the data for training machine learning are most likely imbalanced. Training using the imbalanced data directly leads to more weights assigned to the major class. As a consequence, ostensibly great results may turn out to be false. Generating synthetic samples is one of the solution. Recently, generative adversarial networks (GANs) combining two deep neural networks are studied to generate additional samples for imbalanced problems [20]–[23]. We propose a FDL method incorporating GAN into random forest algorithm (GAN-RF) with extracted and selected features to monitor the SPS of an AES. In the off-line construction stage, the collected data from an AES model and generated data from GAN are exploited to train the RF model after data preprocessing. In the on-line monitoring stage, the hardware based on field-programmable gate array (FPGA) is implemented for parallel preprocessing and prediction.

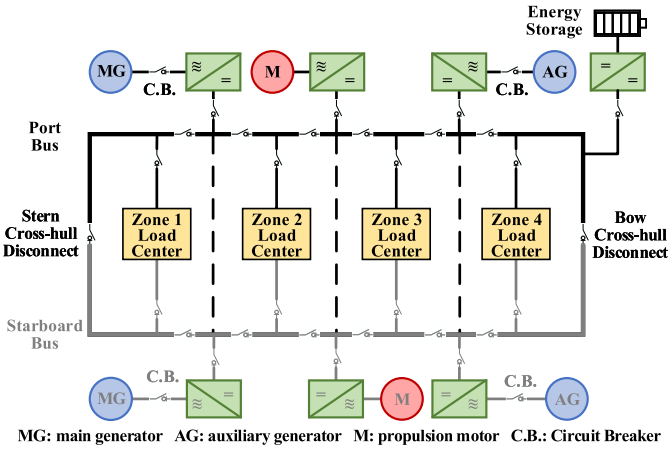

FIGURE 1. Notional ring-bus power system for AES under MVDC [1].

The remainder of this paper is organized as follows. Section II briefly describes the model simulated in PSCAD/EMTDC and selected conditions for diagnosis in the SPS of an AES. Section III elaborates the algorithm preliminaries involved in the proposed GAN-RF method, including generating synthetic samples, feature extraction and selection as well as classification. Section IV presents the discussion of the experimental results including data preparation, feature selection, generated samples, noise resistance and hardware implementation, followed by the conclusions in Section V.

II. MODEL DESCRIPTION

The architecture of a high-performance SPS for the AES fed by MVDC is ring-bus configuration (Fig. 1) as recommended in [1]. Both port and starboard DC buses running longitudinally along the ship can be powered by one main and one auxiliary power generation modules simulated by synchronous generators on each side through bow and stern cross-hull disconnects. A "split-plant" configuration can be set when opening the bow and stern cross-hull disconnect switches. There are four zonal loads from bow to stern along the ship containing different service loads. Critical loads, such as propulsion motors with their modular multilevel converter (MMC) drive inverters, are directly connected to either port or starboard buses through the auto-switches. The low-voltage DC or AC loads in the four zones are supplied by the ring-bus via DC/DC and DC/AC converters and controlled by the circuit breakers. An energy storage system with a bi-directional power capability can provide additional support to meet the quality of service (QoS) requirement. A simplified SPS model with the port-side bus only shown with black-line in Fig. 1 operating in the split-plant configuration is created in PSCAD/EMTDC.

A. SELECTED CONDITIONS

Eleven conditions are simulated by the PSCAD/EMTDC model. There are 1 normal and 10 faulty conditions in total

TABLE 1. Selected Conditions in the Modeled AES System

Location	Descriptions	Conditions
None	No fault	Normal
Main generator	Phase-to-phase short-circuit	Fault1
	Open-circuit in rectifier	Fault2
Auxiliary generator	Phase-to-phase short-circuit	Fault3
	Open-circuit in rectifier	Fault4
Propulsion motor	Phase-to-phase short-circuit	Fault5
	Open-circuit in MMC	Fault6
3-phase AC loads	Phase-to-phase short-circuit of a 450V load in Zone 1	Fault7
	Phase-to-phase short-circuit of a 208V load in Zone 1	Fault8
Energy storage	Short-circuit	Fault9
	Open-circuit in converter	Fault10

that may occur in the components of generators, propulsion motors, converters, loads and buses. The specific locations of the faults are summarized in Table 1. The three types of phase-to-phase short-circuit faults (i.e. A-B, B-C or A-C) in three-phase AC systems are labeled to the same fault class. Minor faults such as open-circuit in diodes of rectifiers and IGBTs of MMC and converter are also selected to be monitored.

III. PRELIMINARIES AND PROPOSED METHOD

In this section, all the algorithms involved in the proposed FDL method for the AES are elaborated. Two stages, including the off-line construction stage and the on-line monitoring stage, for training and testing our intelligent monitoring system are described in detail. In the former stage, features are extracted from the raw time-series data from the simulated model in PSCAD/EMTDC using MEMD. A GAN is designed to generate more valid samples of faulty scenarios based on the training dataset with extracted features to equalize the imbalanced data distribution between normal and faulty conditions. Then samples generated by the GAN model augments the imbalanced ones from PSCAD/EMTDC to become the new balanced training data. Finally, the selected features by CFS embodying both temporal and spectral statistics of the raw data are used to train a RF model that is capable of distinguishing different conditions of the SPS. In the latter stage, the data preprocessing and the constructed RF model are implemented in the FPGA to ensure the evaluation of the system condition can be made in real-time.

A. FEATURE EXTRACTION AND SELECTION

1) FEATURE EXTRACTION BASED ON MEMD

Both temporal and spectral statistics information of the time-series training data are extracted in this work. Temporal features are calculated straightforwardly from the raw signals of training data as following quantities:

$$\mu_t = \frac{1}{N}\sum_{i=1}^{N} x_i, \tag{1}$$

$$\sigma_t = \frac{1}{N-1}\sum_{i=1}^{N} (x_i - \mu_t)^2, \tag{2}$$

where N is the number of time steps of the original time-series signal. μ_t is the mean and σ_t is the variance of a signal.

As for spectral features, signal processing such as EMD is imperative. The EMD decomposes a signal into a set of intrinsic mode functions (IMFs) without leaving the time domain. These IMFs carry different signal components with frequencies ranging from high to low. The decomposition process does not assume the data to be linear and stationary, which is meaningful for analyzing real-world signals. The following algorithm shows the calculation of IMFs from a given signal $x(t)$ step-by-step [24]:

a) Create the upper envelope $e_u(t)$ of all local maxima in $x(t)$ and lower envelope $e_l(t)$ of all local minima using interpolation.

b) From the upper and lower envelopes, get the middle value $m(t) = (e_u(t) + e_l(t))/2$. Then decrease the value of signal by the middle value of the envelope $h_1(t) = x(t) - m(t)$.

c) Check if this extracted signal $h_1(t)$ is an IMF using the standard stopping criterion:

$$0.2 \leq \frac{\sum_{t=0}^{T} \left|h_{1,k-1}(t) - h_{1,k}(t)\right|^2}{\sum_{t=0}^{T} \left|h_{1,k-1}(t)\right|^2} \leq 0.3, \tag{3}$$

d) If $h_1(t)$ is not an IMF, repeat steps a) to c) until an IMF $c_1(t) = h_{1,k}(t)$ is obtained. In each iteration, input the extracted signal instead of $x(t)$ and obtain $h_{1,k}(t)$ in the kth iteration.

e) A residual signal is gained as $r_1(t) = x(t) - c_1(t)$.

f) Repeat steps a) to e) n times with updated input of the last residual signal and obtain $r_n(t)$. At the end of the decomposition, $r_n(t)$ is a monotonic function that cannot be decomposed into an IMF any more. Finally, the original signal can be expressed as:

$$x(t) = \sum_{k=1}^{n} c_k(t) - r_n(t). \tag{4}$$

However, the EMD can only decompose multichannel signals one-by-one without considering the information fusion between different channels. Therefore, a extension variant multivariate EMD (MEMD) is adopted in our case, where multiple voltage and current signals from various components of the SPS in the AES are need to be analyzed. The key concept for MEMD is to find the local mean of n-dimensional multichannel signals by averaging generated n-dimensional envelopes. These envelopes are obtained by projecting signals along different directions in n-dimensional spaces [15]. The results of the MEMD decomposition are several IMFs groups.

The common frequency modes show up in the same order IMFs of different groups.

Two spectral statistics are extracted from IMFs decomposed by MEMD from signals. The strongest center frequency is the first one defined as the center frequency of the order of IMF that has the strongest average power. This feature reflects the dominant frequency band of the signal.

The instantaneous power is the square of amplitude of IMFs given as

$$Q_m(k) = A_m(k)^2. \tag{5}$$

The average power of an IMF is given as

$$\bar{Q}_m = \sum_{k=1}^{N} Q_m(k)/N. \tag{6}$$

The center frequency is defined as

$$\bar{f}_m = \sum_{k=1}^{N} (Q_m(k) \cdot f_m(k)) / \sum_{k=1}^{N} Q_m(k). \tag{7}$$

The strongest center frequency is $f_{\max} = \bar{f}_m$. The mth IMF has the strongest power as

$$\bar{Q}_m = \max\left(\bar{Q}_1, \bar{Q}_2 \cdots \bar{Q}_M\right). \tag{8}$$

The second feature is energy entropy which reflects the uncertainty of energy distribution in frequency domain. The sum of the energies of all the IMFs leaving out the residual should equal to the total energy of the original signal due to the orthogonality of the MEMD, i.e. $E = \sum_{i=1}^{M} E_i$. We define the energy weight of each IMF as $q_i = E_i/E$. Then the energy entropy is expressed as

$$s(q) = -\sum_{i=1}^{M} q_i \ln q_i. \tag{9}$$

2) FEATURE SELECTION BASED ON CFS

As mentioned above, four features (μ_t, σ_t, $f_{\max}$, and $s(q)$) for each signal are extracted from the time-series data. There are 32-channel voltage and current signals in total collected from the SPS of the AES. Therefore, 128 (32×4) features for one sample are required to be reduced and selected from. The selected feature subset with features highly correlated with the class, yet uncorrelated with each other is expected, i.e. irrelevant and redundant features are the target to be eliminated [16]. Correlation-based feature selection (CFS) is a filter method that can pick out representative features according to the correlation among features and class regardless of the machine learning algorithm.

An information theory concept called symmetrical uncertainty is adopted as the correlation measure to estimate the worth of features for classification. For given feature Y and feature (or class) X, the symmetrical uncertainty [16] between them is

$$SU_{X,Y} = 2.0 \cdot \frac{H(Y) + H(X) - H(X,Y)}{H(Y) + H(X)}, \tag{10}$$

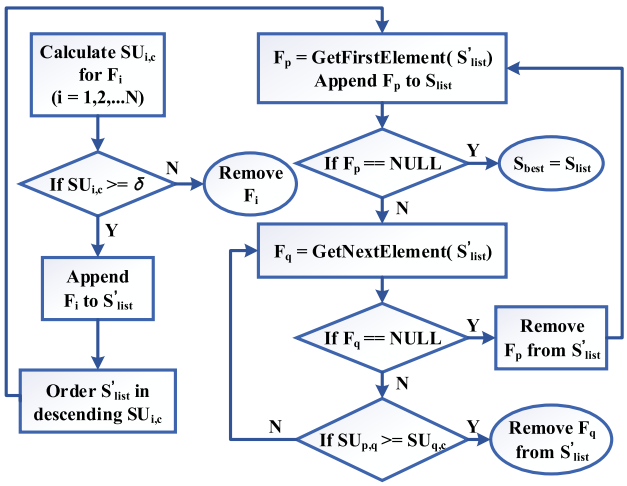

FIGURE 2. Search for the best feature subset using FCBF.

where $H(Y)$ and $H(X)$ are marginal entropy, and $H(X,Y)$ is joint entropy. The definitions [16] are as follows:

$$H(Y) = -\sum_{j} p\left(y_j\right) \log_2\left(p\left(y_j\right)\right), \tag{11}$$

$$H(X,Y) = -\sum_{i}\sum_{j} p\left(x_i, y_j\right) \log_2 p\left(x_i, y_j\right). \tag{12}$$

The value of SU is normalized in the range of 0 to 1. Zero value indicates X and Y are independent, otherwise either one completely depends on the other.

The search approach for the best feature subset using fast correlation-based filter (FCBF) [25] is illustrated in Fig. 2. The value of $SU_{i,c}$ for each feature between the class is calculated. The features with larger value of SU than threshold δ (0.5 in our case) are added into set S'_{list} and ranked in descending order. The first element of S'_{list} (F_p) is regarded as a predominant feature and added to a new set S_{list}. Then subsequent features are checked one-by-one if they are closely associated with F_p via the $SU_{p,q}$ between F_p and F_q. If so, the feature F_q is removed from S'_{list} since it's a redundant peer to F_p. After all features are traversed, the next ranked feature is updated as the new F_p. The iteration continues until all the redundant peers to upper ranked features are removed and S'_{list} is empty. Finally, the best feature subset is selected as S_{list}.

B. GENERATING SAMPLES BASED ON GAN FOR IMBALANCED DATA

The GAN [26] includes two different neural networks (i.e. generator and discriminator), which play a minimax game to find the optimal solution with competitive targets. The goal of the generator is to manufacture samples, having the similar probability distribution with original samples from random inputs, which can deceive the discriminator; while the discriminator is a classifier that should be able to distinguish the fake samples from the real ones. The objective function for

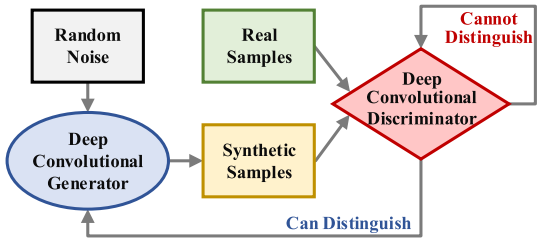

FIGURE 3. Training process of the GAN.

the generator and discriminator can be merged as follows:

$$\min_G \max_D J(D, G) = \mathbb{E}_{x\sim p_{\text{data}}(x)}\left[\log D\left(x\right)\right] + \mathbb{E}_{z\sim p_z(z)}\left[\log\left(1 - D\left(G\left(z\right)\right)\right)\right], \quad (13)$$

where x is the real data and z is the input random noise. $D(x)$ is the output scalar of the discriminator that indicates the possibility of x as real. $G(z)$ is a nonlinear mapping of the generator to data space. The cross-entropy is used to measure the loss. The optimization objective of discriminator is to maximize the likelihood of recognizing the observed data. The first item of the right side of (13) is to recognize the real data better, and the second one is to recognize the fake data better. On the generator side, it wants $D(G(z))$ to earn the highest possibility of $D(x)$ to minimize J while the discriminator is trying to maximize it. Parameters for generator and discriminator are adjusted simultaneously using the gradient-based optimization algorithm (such as Adam [27]) during backpropagation. Fig. 3 displays how GAN is trained.

A popular variant is deep convolutional generative adversarial networks (DCGANs) [28] which is regarded as a basic architecture for most GANs today [29]. The promotions are: 1) batch normalizing most layers of both the generator and discriminator, 2) using all-convolutional net without pooling layers in the overall network, 3) transforming the input dimension of layers via transposed convolution with a stride, and 4) utilizing ReLU and LeakyReLU activation respectively in generator and discriminator for most layers.

In this work, the 128 features extracted from the imbalanced training dataset are first normalized in the range $[-1, 1]$ and regarded as the real inputs of the discriminator with size of $8 \times 16 \times 1$. The fake inputs are generated from 100-dimension random noise by the generator. Two deconvolution layers (having 64 and 32 filters respectively) directly connected to batch normalization layers and filtered by Rectified Linear Unit (ReLU) activation function are adopted. The kernel size of 2 are set to upsample noise inputs to the same size as real inputs. Last convolution layer with tanh activation is to change the channel dimension of the fake inputs into 1. As for the discriminator, two convolution layers with 64, 128 filters are designed to distinguish whether the input is real or fake. The detailed architecture of the generator and discriminator inside GAN is presented in Fig. 4 and the hyper-parameters are listed in Table 2. The parameters for deconvolution and convolution layers represent the number of filters, kernel size and stride respectively. The batch size for training is 256 and the optimizer for both generator and discriminator is Adam [27] with learning rate of 10^{-5} and 10^{-4}.

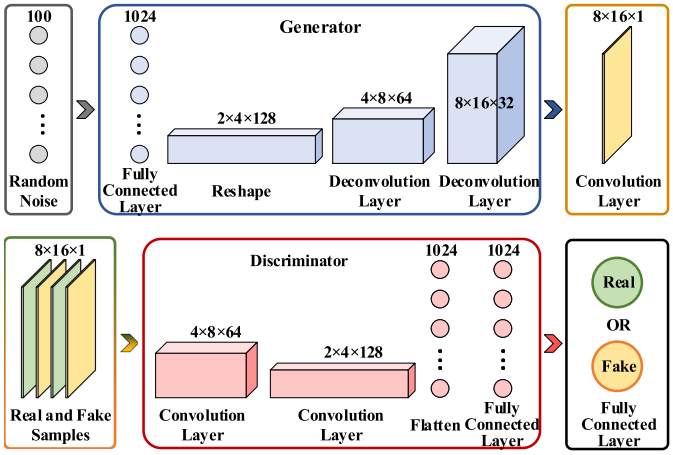

FIGURE 4. Architecture of the deep convolutional generator and discriminator inside GAN.

TABLE 2. Parameters of the Generator and Discriminator Inside GAN

Generator		Discriminator	
Layers	**Parameters**	**Layers**	**Parameters**
Dense	1024	Convolution	(64, 4, 2)
Batch Norm		Leaky ReLU	
ReLU		Convolution	(128, 4, 2)
Reshape	(-1, 2, 4, 128)	Leaky ReLU	
Deconvolution	(64, 4, 2)	Flatten	
Batch Norm		Dense	1024
ReLU		Batch Norm	
Deconvolution	(32, 4, 2)	Leaky ReLU	
Batch Norm		Dense	1
ReLU			
Convolution	(1, 4, 1)		
Tanh			

C. CLASSIFICATION BASED ON RF

Random Forest (RF) is an ensemble learning algorithm that combines multiple weak learners and makes the final decision by vote or average [30]. The single weak learners are comprised of different decision trees. For given training dataset X with N samples and M features, each decision tree T_i is trained using randomly selected m ($m = \log_2 M + 1$) features and N samples with replacement from X (i.e. bootstrap samples). Unpruned trees are grown in accordance to the information gain metric of selected features based on C4.5 methodology [31]. The independent and identical distribution of trees that effectively avoids overfitting is guaranteed by the two random sampling rules for samples and features. In the end, the random forest averages the predictions of individual trees to determine the final classification. Internal unbiased estimate of the generalization error is able to be made since around

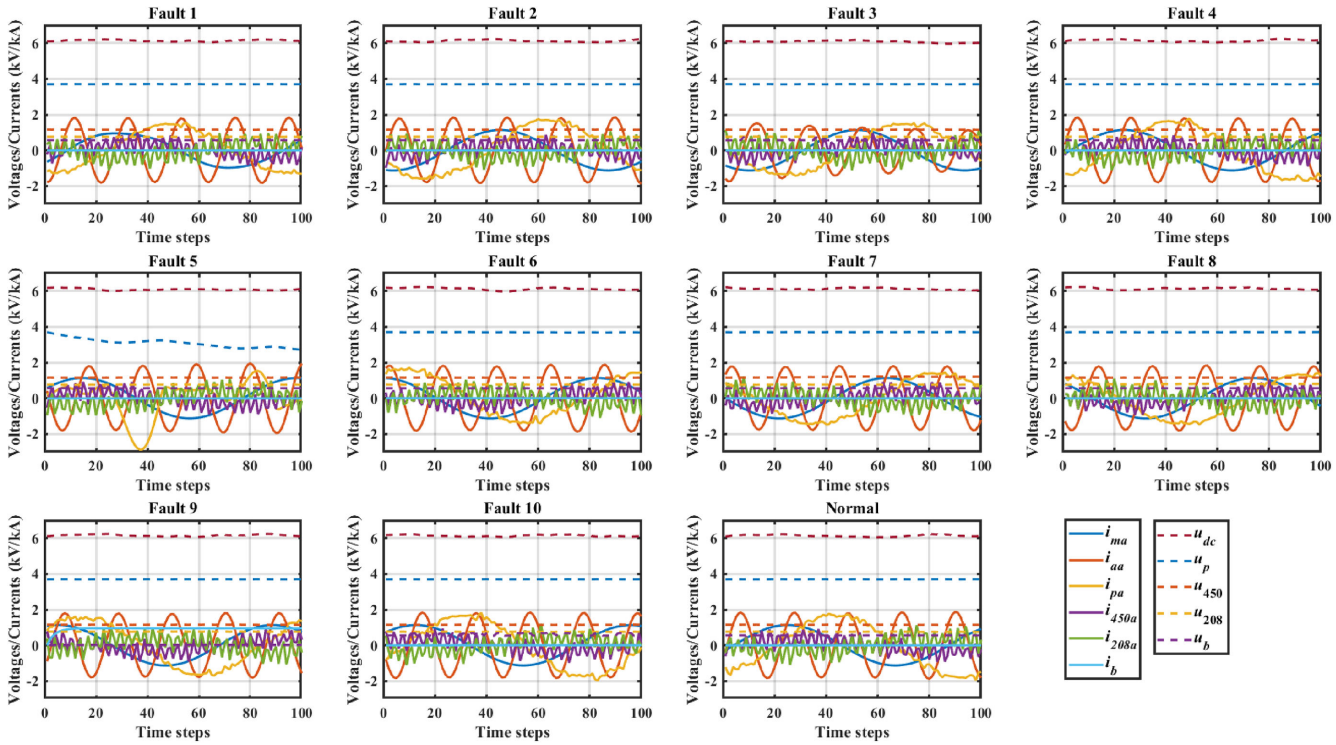

FIGURE 5. Examples of simulation results under different system conditions.

36% samples (called out-of-bag) are not selected during the decision tree building process.

In the on-line monitoring stage, the RF classifier is implemented on the FPGA. The algorithm of RF is suitable for parallel operation since individual trees which are independent with each other can be computed in parallel. Furthermore, only logic operations are executed in the tree model. The input is classified by comparing the feature values with thresholds preset inside the model, i.e. no add, multiply or other complex operations are needed when prediction.

IV. EXPERIMENTAL RESULTS AND DISCUSSION

The proposed GAN-RF method with feature extraction and selection for the FDL in SPS is verified by sufficient number of experiments. Data for training and testing are collected from the established PSCAD/EMTDC model, and training data under faulty conditions for RF model are further generated by the GAN based on existing samples. 11 conditions including 1 normal and 10 faults are simulated and prepared to be distinguished. Real-time FDL implementation of SPS has been carried out on an hardware platform consisting of the Xilinx XCVU37P FPGA. Data preparation and experiment results are elaborated in this section.

A. DATA PREPARATION

The established model in PSCAD/EMTDC provides the dataset for FDL monitoring system to be trained and tested. In order to simulate faulty conditions, faults are injected to the system after it reaches the steady-state. The start time of sampling is at the fault injected time point which randomly distributed at any point among one specific period of the system after stabilization considering the differences when a fault occurs at different points of an AC period. There are 32-channel voltage and current signals for each sample and 100 time steps with sampling frequency of 5 kHz are collected for each signal. For training, 600 samples under the normal condition and 100 samples under each faulty conditions are obtained. Another 150 samples for each one of the 11 conditions are prepared for testing. The simulation results of part current and voltage signals of randomly selected samples for each system condition are depicted in Fig. 5. It is clear that the curves are very similar in the 100-time-step range, so the difficulty of classifying each other in a very short time directly from the raw time-series dataset can be imagine.

B. FEATURE EXTRACTION AND SELECTION

The aforementioned 4 features (i.e. μ_t, σ_t, $f_{\max}$, and $s(q)$) are extracted from each signal. For one sample, there are 128 features in total after feature extraction using MEMD since 32-channel raw signals are sampled from the simulated model. The description of each signal is listed in Table 3. The IMFs of three signals decomposed by MEMD are presented in Fig. 6. Finally, 50 features bold in Table 3 are selected as the best feature subset based on CFS. The parenthesis behind a signal tab represents the extracted features based on that signal: M for mean, V for variance, F for strongest center frequency, and E for energy entropy.

TABLE 3. Signals for Each Sample Collected From Simulated Model

Location	Signals	Tabs
Main generator	Current on phase A	i_{ma} **(V)**
	Current on phase B	i_{mb} **(F)**
	Current on phase C	i_{mc}
	Three-phase RMS voltage	u_{m1} **(M, V, E)**
	Output current of ACDC	i_{dc1} **(E)**
	Voltage on port bus	u_{dc} **(V)**
Auxiliary generator	Current on phase A	i_{aa} **(V)**
	Current on phase B	i_{ab} **(V)**
	Current on phase C	i_{ac} **(V)**
	Three-phase RMS voltage	u_{m2} **(M, V, F)**
	Output current of ACDC	i_{dc2} **(M)**
Propulsion motor	Current on phase A	i_{pa}
	Current on phase B	i_{pb}
	Current on phase C	i_{pc}
	Three-phase RMS voltage	u_p **(M, V, F, E)**
	Input current of DCAC	i_{dcp} **(M, V, F)**
450VAC load	Current on phase A	i_{450a} **(V)**
	Current on phase B	i_{450b}
	Current on phase C	i_{450c} **(V, F)**
	Three-phase RMS voltage	u_{450rms} **(E)**
	Input current of DCDC	i_{dc450} **(F)**
	Output current of DCDC	i_{450} **(M, V)**
	Output voltage of DCDC	u_{450} **(M, V, F, E)**
208VAC load	Current on phase A	i_{208a}
	Current on phase B	i_{208b} **(V)**
	Current on phase C	i_{208c} **(V, F)**
	Three-phase RMS voltage	u_{208rms} **(V, E)**
	Input current of DCDC	i_{dc208}
	Output current of DCDC	i_{208} **(M, V, F, E)**
	Output voltage of DCDC	u_{208} **(V, F, E)**
Energy storage	Current	i_b **(M, V, F, E)**
	Voltage	u_b **(M, F)**

The bold ones are the selected signals.
The symbols in the parenthesis represent the extracted features based on the signal: M for mean, V for variance, F for strongest center frequency, and E for energy entropy.

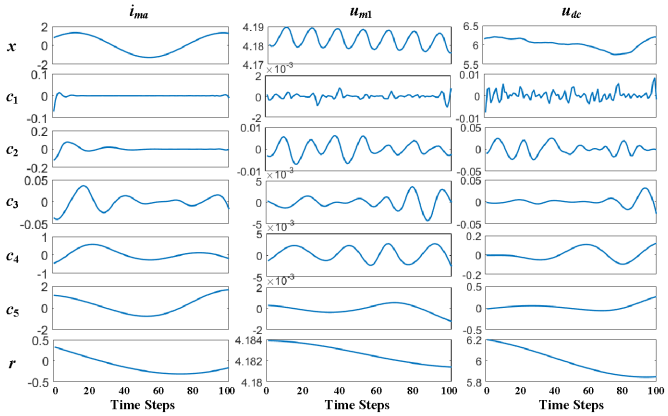

FIGURE 6. IMFs of three signals decomposed by MEMD.

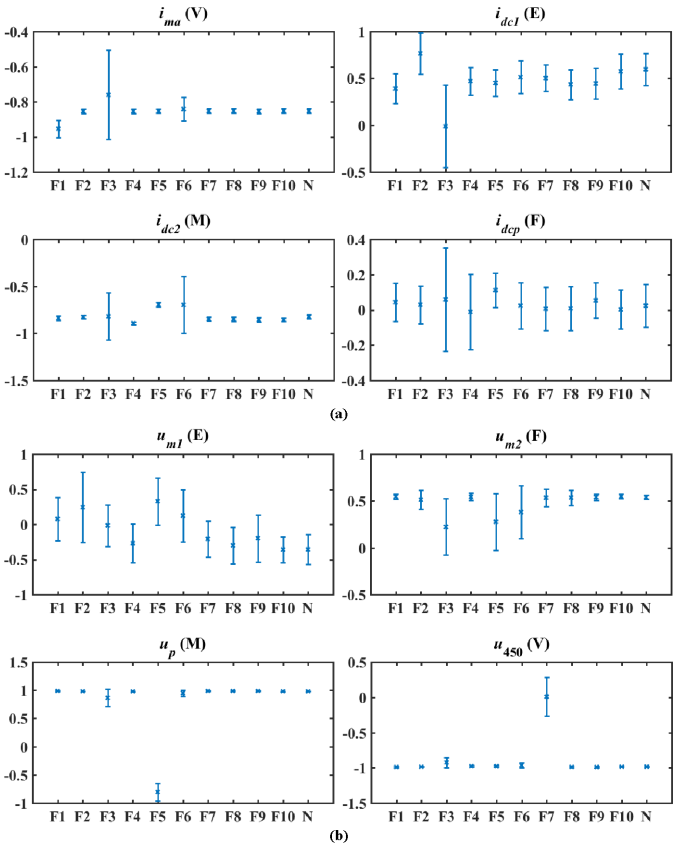

FIGURE 7. Statistical analysis of features under 11 conditions.

Statistical analysis of the 8 examples in 50 current and voltage features are summarized in Fig. 7(a) and (b). Each diagram shows the mean value and standard deviation of the specific feature in the training dataset under 11 different system conditions. On the one hand, it indicates the rationality and effectiveness of the extracted and selected features since these feature distributions between different system conditions are diverse compared with Fig. 5, and some of the faults can be easily distinguished only by a few features. For instance, the mean of u_p in Fault 5 and the variance of u_{450} in Fault 7 are distinct from others. On the other hand, it also manifests the necessity of a machine learning based classifier which has the capability of learning the inherent rules from these enormous and complicated feature distributions automatically and then making correct evaluation of the system condition from testing dataset timely.

C. GENERATED SAMPLES

One of the challenges for industrial fault detection using machine learning methods, as in our case, is that it is hard to obtain the balanced dataset since the data of faulty conditions are commonly far fewer than that for the normal condition. Training the imbalanced data directly causes more weights assigned to the major class and further leads to lower the accuracy of fault classification. Therefore, we exploit GAN network to generated more samples to augment our dataset. There are no universal metrics to evaluate the quality of the generated data using GAN. Various metrics including inception score and frechet distance are monitoring during training.

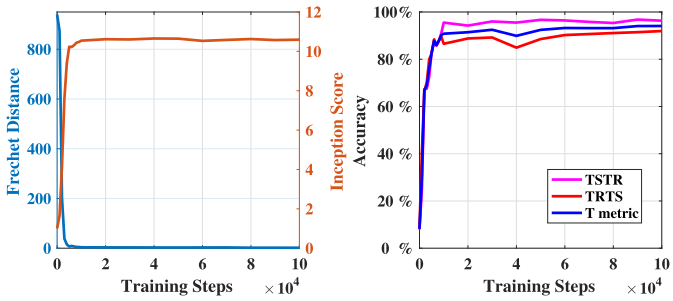

FIGURE 8. Change of metrics along GAN training steps.

Finally, the T metric [32], as defined in (14), combining two empirical evaluation metrics: TSTR (Train on Synthetic Test on Real) and TRTS (Train on Real Test on Synthetic) is introduced to determine the eligible synthesized data to train the FDL monitor model:

$$T = \frac{2 \cdot TSTR \cdot TRTS}{TSTR + TRTS}. \tag{14}$$

We summarize the metrics changing along GAN training steps in Fig. 8. From the left side figure, it's clear that the score and distance tend to converge at stable points after 10,000 steps. Synthesized dataset of different training steps from the generator are collected, and then RF method with CFS feature selection are applied between real dataset simulated from PSCAD/EMTDC and synthesized dataset generated by GAN network to calculate the TSTR and TRTS metrics. As shown in the right side figure, TSTR and TRTS reaches a high accuracy quickly for the first 10,000 steps, and then keep growing gradually. After 100,000 training steps, they are able to achieve the accuracy of around 96% and 91% respectively. Finally, the best generated dataset is picked out according to the T metric by trial and error. The distribution of four features at different training steps (10000, 50000 and 100000 respectively) between real and fake data are compared in Fig. 9. Different colors stand for different classes (fault types). It displays the number of samples (vertical ordinate) of each class located at a small range of specific values (horizontal ordinate). It proves that the GAN network can learn the distribution of the real dataset well with training steps increasing.

D. NOISE RESISTANCE

We test the anti-noise capability of the proposed GAN-RF method by adding different level of noise to the testing dataset. The signals-to-noise ratios (SNRs) of 90, 70, 50, 30 and 10 dB are introduced. In this experiment, we augment the simulated training dataset from PSCAD/EMTDC by adding 500 more samples generated by GAN for each faulty condition. Therefore, the training dataset is balanced now with 600 samples for each one of the 11 conditions. Then the RF method with CFS feature selection is applied to classify the real testing dataset with noise. The fault detection accuracy of the monitor with different noise level using both imbalanced and augmented dataset to train the RF model is presented in Fig. 10. It proves that the GAN-RF based FDL method can resist the noise to certain extent since the samples from GAN in the training dataset include noise naturally. Only when the noise level reaches a very high level, for instance, when the SNR is less than 50 dB, the judgment of monitors may be unreliable. However, it would not be normal for sensors to contain such high-level noise. In addition, it is obvious that the accuracy is improved from 96% (the TSTR result) to 99% combining real data while training. In the TSTR experiments, many errors occur when distinguishing the differences between the normal condition and minor faults. However, in the augmented dataset, all of the samples for the normal condition are the real data. Therefore, the real data must help with correction of the RF model which explains the improvement of the accuracy.

E. REAL-TIME HARDWARE IMPLEMENTATION

The data preprocessing and constructed RF model are implemented on the FPGA to ensure the evaluation of the system condition of the SPS can be made in real-time. The highly parallel hardware architecture of FPGA matches well with the structure of the random forest model, and also helps to optimize the execution time of the data preprocessing.

The real-time monitoring system is implemented on the Xilinx Virtex UltraScale+^{TM} VCU128 FPGA board [33], which provides the hardware environment for designs targeting the Virtex UltraScale+^{TM} XCVU37P HBM FPGA with 2,852,000 programmable logic cells, 340.9Mb BRAM, and 9,024 DSP slices. The hardware platform for the on-line testing experiment is presented in Fig. 11. The testing dataset simulated and collected from PSCAD/EMTDC are saved in the host PC which served as a real-time AES SPS model. It outputs the time-series signals and communicates with the FPGA monitor through PCIe 3.0 interface, while the FPGA monitor updates the evaluation result of the system condition with refreshed data. The oscilloscope displays the waveforms of input signals and output results.

Thanks to the high-level synthesis (HLS) technology [34], the development cycle of a new FPGA hardware implementation has been greatly reduced. The designer can concentrate more on the algorithm itself by exploiting high-level programming languages such as C/C++ rather than focusing on the low-level details of hardware development using hardware description languages (HDL). In this work, the algorithms of preprocessing and RF are written with C++ language. Then the codes with Q8.24 fixed-point data precision and optimization directives for parallel hardware implementation, such as pipeline, unroll, array partition and so forth, are synthesized by HLS automatically and packaged as user-designed IP core. Finally, the bitstream file is obtained after synthesis, implementation, bitstream generation processes, and programmed to the FPGA board. The latency and resource consumption on the FPGA for both data preprocessing and RF model are summarized in Table 4. The latency and resources required by RF model are significantly small compared with those for preprocessing due to its inherently parallel structure and logic

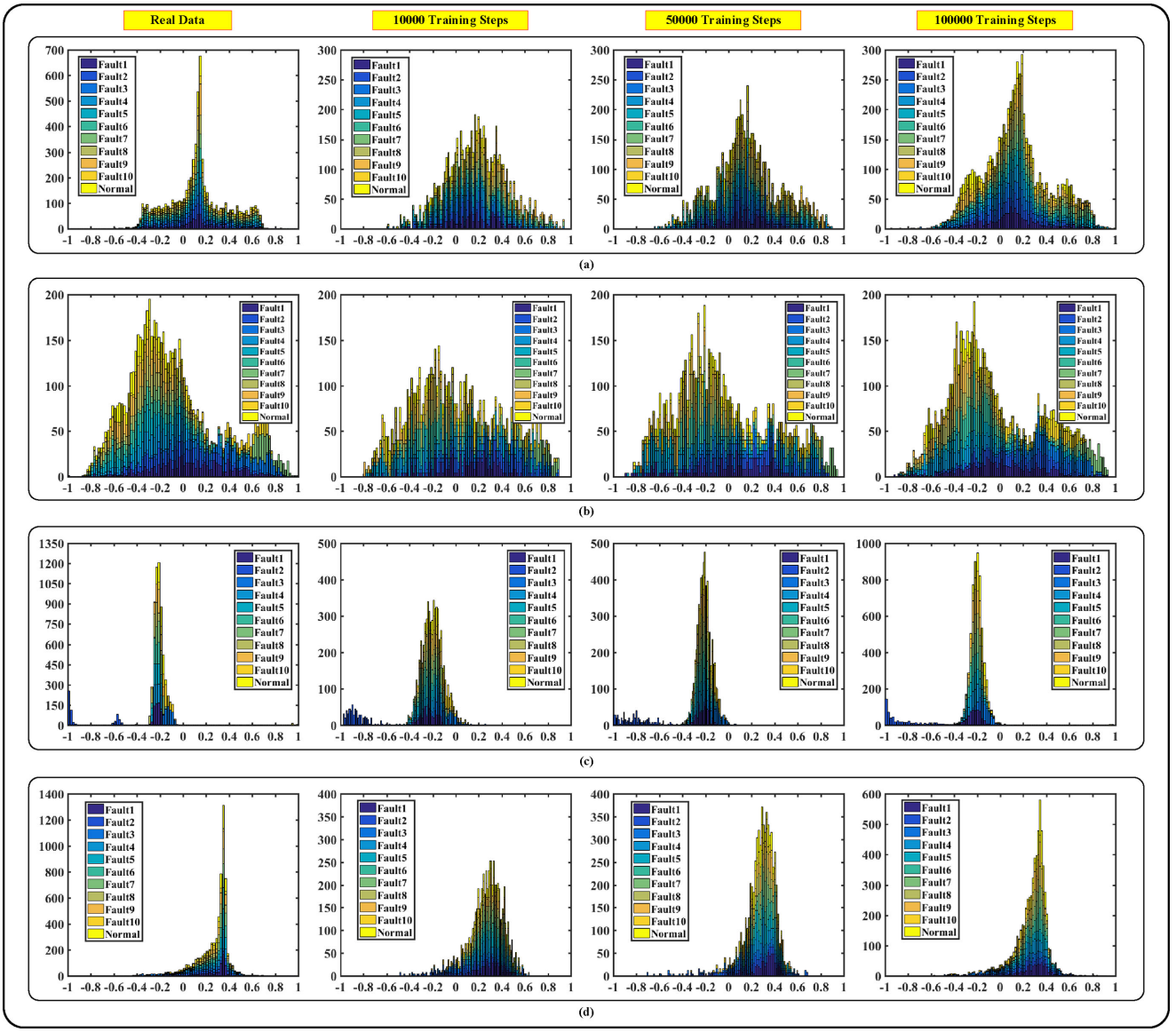

FIGURE 9. Comparison of feature distributions between real and fake data for: (a) the strongest center frequency of i_{mb}, (b) the energy entropy of u_{m1}, (c) the variance of i_{ac}, (d) the strongest center frequency of u_p.

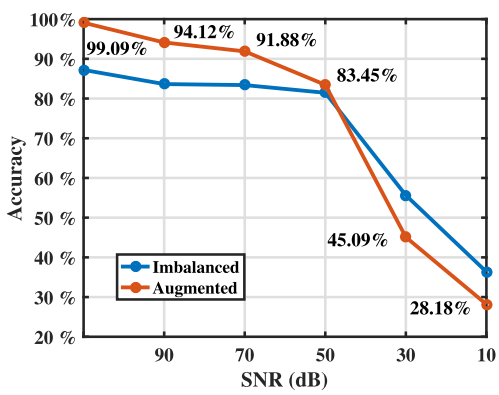

FIGURE 10. Classification accuracy under different noise levels.

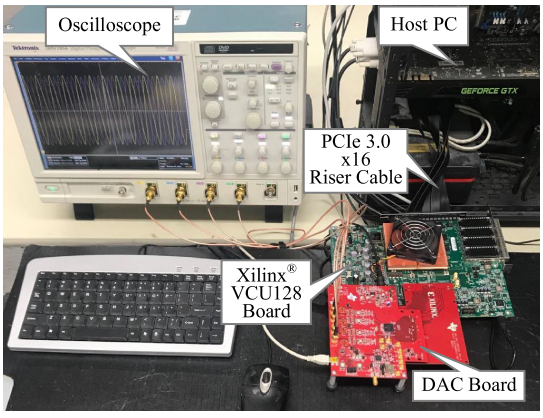

FIGURE 11. Hardware platform configuration used in the on-line testing experiment for the FDL monitoring system of AES SPS.

TABLE 4. Latency and Resource Consumption of Hardware Implementation on the Xilinx XCVU37P FPGA

	BRAM	DSP	FF	LUT	Latency(ms)
Pre-processing	667	785	870689	1104934	5.76
Random forest	4	0	1579	5869	6.40×10^{-4}
Total	15%	8%	33%	84%	5.76

operations used inside rather than other complex operations. The total latency for calculating a 100-step sample is around 6 ms within which the breakers can successfully cut off the fault circuit [35].

V. CONCLUSION

In this paper, an FDL method was proposed to monitor the SPS condition of the AES based on the GAN-RF method in real-time. In accordance to the fact that considerably fewer data under faulty conditions than those under the normal condition are available in real-world industry, GAN network was explored to generate more valid samples and then augment the training dataset for RF classifier. The entire SPS was established in PSCAD/EMTDC which was used to simulate different normal or faulty conditions of the system. Both training and testing time-series dataset were collect from the simulated model. Then the temporal and spectral statistics information of these raw data were extracted using MEMD. From the experiment result, GAN network was proved to have the capability of learning the distribution of these extracted features. Feature selection method CFS was conducted to further reduce the number of features for each sample. Finally, the experimental results manifested that the RF classifier, trained by the augmented training dataset which combines imbalanced data from simulated model and generated data by GAN, could reach 99% accuracy of classifying 11 conditions of the SPS with excellent anti-noise capability. Additionally, the real-time monitoring including preprocessing and prediction could be achieved within 6 ms by hardware implementation on the FPGA. Although 11 conditions were selected as examples to validate the proposed FDL method, other scenarios, such as normal conditions with different loads and faulty conditions that are unknown or unlabeled, will be further explored in our future work.

REFERENCES

[1] "*IEEE Recommended Practice for 1 kV to 35 kV Medium-Voltage DC Power Systems on Ships*," IEEE Standard 1709-2018 (Revision of IEEE Standard 1709-2010), pp. 1–54, Dec 2018.

[2] Q. Xu, B. Yang, Q. Han, Y. Yuan, C. Chen, and X. Guan, "Optimal power management for failure mode of MVDC microgrids in all-electric ships," *IEEE Trans. Power Syst.*, vol. 34, no. 2, pp. 1054–1067, Mar. 2019.

[3] U. Javaid, F. D. Freijedo, W. Merwe, and D. Dujic, "Stability analysis of multi-port MVDC distribution networks for all-electric ships," *IEEE Trans. Emerg. Sel. Top. Power Electron.*, vol. 8, no. 2, pp. 1164–1177, Jun. 2020.

[4] K. P. Logan, "Intelligent diagnostic requirements of future all-electric ship integrated power system," *IEEE Trans. Ind. Appl.*, vol. 43, no. 1, pp. 139–149, Jan.\Feb. 2007.

[5] T. Pan, J. Chen, Z. Zhou, C. Wang, and S. He, "A novel deep learning network via multiscale inner product with locally connected feature extraction for intelligent fault detection," *IEEE Trans. Ind. Inform.*, vol. 15, no. 9, pp. 5119–5128, Sep. 2019.

[6] K. Zhong, M. Han, T. Qiu, B. Han, and Y. Chen, "Distributed dynamic process monitoring based on minimal redundancy maximal relevance variable selection and Bayesian inference," *IEEE Trans. Control Syst. Technol.*, vol. 28, no. 5, pp. 2037–2044, Sep. 2020.

[7] J. Zhou, Y. Yang, S. X. Ding, Y. Zi, and M. Wei, "A fault detection and health monitoring scheme for ship propulsion systems using SVM technique," *IEEE Access*, vol. 6, pp. 16207–16215, 2018.

[8] B. Chang, R. Yang, C. Guo, S. Ge, and L. Li, "A new application of optimized random forest algorithms in intelligent fault location of rudders," *IEEE Access*, vol. 7, pp. 94276–94283, 2019.

[9] W. Gao, R. Wai, S. Qiao, and M. Guo, "Mechanical faults diagnosis of high-voltage circuit breaker via hybrid features and integrated extreme learning machine," *IEEE Access*, vol. 7, pp. 60091–60103, 2019.

[10] X. Wang *et al.*, "High impedance fault detection method based on variational mode decomposition and teagerkaiser energy operators for distribution network," *IEEE Trans. Smart Grid*, vol. 10, no. 6, pp. 6041–6054, Nov. 2019.

[11] M. Mishra and P. K. Rout, "Detection and classification of micro-grid faults based on HHT and machine learning techniques," *IET Gener., Transmiss. Distrib.*, vol. 12, no. 2, pp. 388–397, 2018.

[12] X. Wang, J. Gao, X. Wei, Z. Zeng, Y. Wei, and M. Kheshti, "Single line to ground fault detection in a non-effectively grounded distribution network," *IEEE Trans. Power Del.*, vol. 33, no. 6, pp. 3173–3186, Dec. 2018.

[13] L. Mengting, H. Darong, Z. Ling, C. Ruyi, F. Kuang, and J. Yu, "An improved fault diagnosis method based on a genetic algorithm by selecting appropriate IMFs," *IEEE Access*, vol. 7, pp. 60310–60321, 2019.

[14] H. Zhang, Z. Feng, and J. Zou, "Research on feature extraction and pattern recognition of acoustic signals based on MEMD and approximate entropy," in *Proc. 29th China Control Decis. Conf.*, May 2017, pp. 4844–4849.

[15] N. Rehman and D. Mandic, "Multivariate empirical mode decomposition," in *Proc. Roy. Soc. A*, 2010, vol. 466, pp. 1291–1302.

[16] M. A. Hall, "Correlation-based feature selection for discrete and numeric class machine learning," in *Proc. 17th Int. Conf. Mach. Learn.*, 2000, pp. 359–366.

[17] D. Li, Y. Zhou, G. Hu, and C. J. Spanos, "Optimal sensor configuration and feature selection for AHU fault detection and diagnosis," *IEEE Trans. Ind. Informat.*, vol. 13, no. 3, pp. 1369–1380, Jun. 2017.

[18] T. Kari *et al.*, "Hybrid feature selection approach for power transformer fault diagnosis based on support vector machine and genetic algorithm," *IET Gener., Transmiss. Distrib.*, vol. 12, no. 21, pp. 5672–5680, 2018.

[19] A. U. Haq, D. Zhang, H. Peng, and S. U. Rahman, "Combining multiple feature-ranking techniques and clustering of variables for feature selection," *IEEE Access*, vol. 7, pp. 151482–151492, 2019.

[20] S. Lu, T. Sirojan, B. T. Phung, D. Zhang, and E. Ambikairajah, "DA-DCGAN: An effective methodology for DC series arc fault diagnosis in photovoltaic systems," *IEEE Access*, vol. 7, pp. 45831–45840, 2019.

[21] C. Ren and Y. Xu, "A fully data-driven method based on generative adversarial networks for power system dynamic security assessment with missing data," *IEEE Trans. Power Syst.*, vol. 34, no. 6, pp. 5044–5052, Nov. 2019.

[22] W. Mao, Y. Liu, L. Ding, and Y. Li, "Imbalanced fault diagnosis of rolling bearing based on generative adversarial network: A comparative study," *IEEE Access*, vol. 7, pp. 9515–9530, 2019.

[23] W. Jiang, Y. Hong, B. Zhou, X. He, and C. Cheng, "A GAN-based anomaly detection approach for imbalanced industrial time series," *IEEE Access*, vol. 7, pp. 143608–143619, 2019.

[24] N. E. Huang *et al.*, "The empirical mode decomposition and the Hilbert spectrum for nonlinear and non-stationary time series analysis," *Proc. Roy. Soc. Lond. A.*, 1998, vol. 454, pp. 903–995, Mar.

[25] L. Yu and H. Liu, "Feature selection for high-dimensional data: A fast correlation-based filter solution," in *Proc. 20th Int. Conf. Mach. Learn.*, 2003, vol. 2, pp. 856–863.

[26] I. Goodfellow *et al.*, "Generative adversarial networks," in *Proc. Int. Conf. Neural Inf. Process. Syst.*, 2014, pp. 2672–2680.

[27] D. P. Kingma and J. Ba, "Adam: A method for stochastic optimization," 2014. [Online]. Available: https://arxiv.org/abs/1412.6980
[28] A. Radford, L. Metz, and S. Chintala, "Unsupervised representation learning with deep convolutional generative adversarial networks," 2015. [Online]. Available: https://arxiv.org/abs/1511.06434
[29] I. Goodfellow, "NIPS 2016 tutorial: Generative adversarial networks," 2016. [Online]. Available: https://arxiv.org/abs/1701.00160
[30] L. Breiman, "Random forests," *Mach. Learn.*, vol. 45, pp. 4–32, Oct. 2001.
[31] J. R. Quinlan, *C4.5: Programs for Machine Learning*, (Morgan Kaufmann series in machine learning). New York, NY, USA: Elsevier Science, 1993.
[32] K. Nikolaidis *et al.*, "Augmenting physiological time series data: A case study for sleep apnea detection," 2019. [Online]. Available: http://arxiv.org/abs/1905.09068
[33] Xilinx, "VCU128 evaluation board user guide," 2018. [Online]. Available: https://www.xilinx.com/support/documentation/boards_and_kits/vcu128/ug1302-vcu128-eval-bd.pdf
[34] Xilinx, "Vivado design suite user guide: High-level synthesis," 2014. [Online]. Available: https://www.xilinx.com/support/documentation/sw_manuals/xilinx2018_3/ug902-vivado-high-level-synthesis.pdf
[35] A. Rojek, "Parameters of DC high-speed circuit-breakers," in *Proc. 13th Int. Conf. MET*, Jul. 2018, pp. 1–5.

QIN LIU (Student Member, IEEE) received the B.Eng. degree in measurement and control technology and instrument from Beijing Jiaotong University, Beijing, China, in 2013. She is currently working toward the Ph.D. degree with the School of Mechanical, Electronic and Control Engineering, Beijing Jiaotong University and being a Visiting Ph.D. Student with Electrical and Computer Engineering, the University of Alberta, Edmonton, Alberta, Canada. Her research interests include real-time simulation and control of power systems, hardware acceleration, and system-on-chip.

TIAN LIANG (Member, IEEE) received the B.Eng. degree in electrical engineering from Nanjing Normal University, Nanjing, Jiangsu, China, in 2011, the M.Eng. degree from Tsinghua University, Beijing, China, in 2014, the Ph.D. degree in energy systems from the University of Alberta, Edmonton, AB, Canada, in 2020. His research interests include real time simulation of power systems, power electronics, a rtificial intelligence field programmable gate arrays, and system on chip.

VENKATA DINAVAHI (Fellow, IEEE) received the B.Eng. degree in electrical engineering from the Visveswaraya National Institute of Technology, Nagpur, India, in 1993, the M.Tech. degree in electrical engineering from the Indian Institute of Technology, Kanpur, India, in 1996, and the Ph.D. degree in electrical and computer engineering from the University of Toronto, Ontario, Canada, in 2000. He is currently a Professor with the Department of Electrical and Computer engineering, University of Alberta, Edmonton, Alberta, Canada. His research interests include real-time simulation of power systems and power electronic systems, electromagnetic transients, device-level modeling, large-scale systems, and parallel and distributed computing.